Development of an adenosquamous carcinoma histopathology - selective lung metastasis model

Lähdeniemi, Iris Aino Karoliina

2022

Lähdeniemi , I A K , Devlin , J , Nagaraj , A , Talwelkar , S , Bao , J , Linnavirta , N M M , Seref Vujaklija , C , Kiss , E A , Hemmes , A & Verschuren , E 2022 , ' Development of an adenosquamous carcinoma histopathology - selective lung metastasis model ' , Biology open , vol. 11 , no. 12 , bio059623 . https://doi.org/10.1242/bio.059623

http://hdl.handle.net/10138/355203
https://doi.org/10.1242/bio.059623

© 2022. Published by The Company of Biologists Ltd | Biology Open (2022) 11, bio059623. doi:10.1242/bio.059623

RESEARCH ARTICLE

Development of an adenosquamous carcinoma histopathology – selective lung metastasis model

Iris A. K. Lähdeniemi[1,*], Jennifer R. Devlin[1,*], Ashwini S. Nagaraj[1], Sarang S. Talwelkar[1], Jie Bao[1], Nora Linnavirta[1], Ceren Şeref Vujaklija[1], Elina A. Kiss[2], Annabrita Hemmes[1] and Emmy W. Verschuren[1,‡]

ABSTRACT

Preclinical tumor models with native tissue microenvironments provide essential tools to understand how heterogeneous tumor phenotypes relate to drug response. Here we present syngeneic graft models of aggressive, metastasis-prone histopathology-specific NSCLC tumor types driven by *KRAS* mutation and loss of *LKB1* (KL): adenosquamous carcinoma (ASC) and adenocarcinoma (AC). We show that subcutaneous injection of primary KL; ASC cells results in squamous cell carcinoma (SCC) tumors with high levels of stromal infiltrates, lacking the source heterogeneous histotype. Despite forming subcutaneous tumors, intravenously injected KL;AC cells were unable to form lung tumors. In contrast, intravenous injection of KL;ASC cells leads to their lung re-colonization and lesions recapitulating the mixed AC and SCC histopathology, tumor immune suppressive microenvironment and oncogenic signaling profile of source tumors, demonstrating histopathology-selective phenotypic dominance over genetic drivers. Pan-ERBB inhibition increased survival, while selective ERBB1/EGFR inhibition did not, suggesting a role of the ERBB network crosstalk in resistance to ERBB1/EGFR. This immunocompetent NSCLC lung colonization model hence phenocopies key properties of the metastasis-prone ASC histopathology, and serves as a preclinical model to dissect therapy responses and metastasis-associated processes.

KEY WORDS: NSCLC, Adenosquamous carcinoma, Histopathology, Metastasis, Lung colonization, Preclinical model

INTRODUCTION

Non-small cell lung cancer (NSCLC) is the most common form of lung cancer (85%) and one of the leading cancer-related causes of deaths in the world. NSCLC is a heterogeneous disease that is often discovered at late stages resulting in poor prognoses and clinical outcomes (Bray et al., 2018). Novel tyrosine kinase inhibitors (TKIs) and immunotherapy agents have provided significant clinical promise for NSCLC treatment in the past decade with approved TKIs such as erlotinib and afatinib demonstrating increased progression-free survival compared to conventional chemotherapy (Liu et al., 2021). Immunotherapy with programmed cell death 1 (PD-L1) checkpoint inhibitors is approved for metastatic NSCLC treatment and significantly increases patient survival rates (Brahmer et al., 2015). However, heterogeneity of immune checkpoint protein expression is a feature of NSCLC that limits the broad effectiveness of these therapies (Gettinger et al., 2015), with the absence of PD-L1 expression identified in both human and murine tumors with oncogenic *KRAS* and loss-of-function *LKB1* mutations (Calles et al., 2015; Koyama et al., 2016; Skoulidis et al., 2015). The absence of checkpoint marker expression in pre clinical models of *KRAS*;*LKB1* mutant NSCLC corresponded with poor to no responsiveness to checkpoint immunotherapy, and effective treatments to durably target tumors that are non-responsive to immunotherapy or TKIs remain lacking (Skoulidis et al., 2018; Li et al., 2022).

Genetically engineered mouse models (GEMMs) constitute excellent tools to model the diversity of NSCLC biology, allowing assessment of therapeutic responses within the context of native immunocompetent microenvironments. Our previous findings highlight the importance of the cell-of-origin in histotype-selective growth of tumors driven by oncogenic $Kras^{G12D}$ mutation and loss of *Lkb1* (KL). Tumors initiated in club cell antigen 10 (CC10) progenitors led to predominant formation of mixed histopathology adenosquamous carcinoma (ASC) tumors and a wider range of histotypes compared to KL tumors originating from surfactant protein C (SPC) progenitors that predominantly exhibited adenocarcinoma (AC) histopathology (Nagaraj et al., 2017). Interestingly, KL;ASC tumors exhibited a histotype-selective immune suppressive microenvironment with decreased expression of MHC genes and decreased T-cell infiltration, as well as increased recruitment of $CD11b^{+}$ $GR1^{+}$ tumor-associated-neutrophils (TANs) (Nagaraj et al., 2017; Schabath et al., 2016).

GEMMs have served as a great tool to study cancer biology including localized progression and distal metastasis, which are both influenced by multiple factors including the immune system, the tumor microenvironment (TME) and driver genes. GEMM studies have contributed to development of novel therapeutics with efficacy for specific subsets of NSCLC, such as TKIs, as well as other targeted and immunotherapies (Yuan et al., 2019). Despite their advantages to dissect disease pathology, the extended time frames for tumor development as well as intra- and inter-cohort heterogeneity limits the utility of GEMMs for accelerated evaluation of anti-cancer drug efficacy. While advances have been made for the establishment of faithful *in vitro* and *ex vivo* approaches to model both patient- and GEMM-derived tumors, these models exhibit limitations in their ability to fully recapitulate the complexities of *in vivo* tumor biology and consequently to optimally reflect therapeutic responses (Chaffer and Weinberg, 2011; Quinn et al., 2021).

To address methodological limitations in evaluation of cancer treatment approaches, we and others have developed and validated

[1]Institute for Molecular Medicine Finland (FIMM), HiLIFE, University of Helsinki, Helsinki, Finland. [2]University of Helsinki and Wihuri Research Institute, Helsinki, Finland.
*Co-first authors

‡Author for correspondence (emmy.verschuren@helsinki.fi)

E.W.V., 0000-0001-5771-9129

Received 6 September 2022; Accepted 2 November 2022

Biology Open (2022) 11, bio059623. doi:10.1242/bio.059623

methods for NSCLC functional diagnostics, including conditionally reprogrammed cells (CRCs) (Liu et al., 2012), long-term 3D organoid culture (Kim et al., 2019; Sachs et al., 2019) and analysis of functional uncultured tumor cells (FUTCs) (Talwelkar et al., 2021). These *ex vivo* models can complement GEMMs in preclinical cancer research. For example, culture and analysis of KL GEMM-derived primary cells specifically uncovered NSCLC histotype-selective drug sensitivity and bypass resistance mechanism. MEK inhibitor (trametinib) treatment was shown to be selective for AC tumors, while both ASC and AC histotypes showed response to the pan-ERBB inhibitor afatinib. *Ex vivo* data was validated *in vivo,* showing afatinib response in both KL;ASC and KL;AC tumors (Talwelkar et al., 2019).

GEMMs exhibit limitations as preclinical models due to relatively long tumor development times as well as inter-tumor histotype diversity between mice within treatment cohorts. We here set out to develop subcutaneous (s.c.) and intravenous (i.v.) transplantation models to study KL;ASC and -AC histotype tumors in both immune-competent and -compromised hosts. We observed differential metastatic capacity of histotype-selective cells, unexpectedly showing that only ASC cells were capable of re-colonizing the lung after i.v. transplantation. Importantly, these lung colonized tumors retained the key mixed AC and SCC histotype features as well as immunosuppressive TME of source ASC tumors, which was not seen with the s.c. model. We analyzed responses to inhibitors of ERBB family receptor tyrosine kinases (RTKs) that have been previously shown to drive tumor progression in the KL GEMM, and found that only pan-ERBB inhibition increased the survival of $ASC^{i.v.}$ mice compared to control or single ERBB1/EGFR inhibition. Taken together, this syngeneic $ASC^{i.v.}$ transplantation model will be useful to evaluate therapy responses in microenvironments that accurately recapitulate GEMM biology, and will help to analyze the mechanisms behind the differential metastatic capacity of ASC tumor cells.

RESULTS

Development of a NSCLC metastatic lung cancer model

Our previous studies in mice have revealed that selective expression of the oncogenic $Kras^{G12D}$ allele in combination with *Lkb1* deletion (KL) in lung CC10 cells leads to formation of aggressive ASC lesions, in addition to other tumor histotypes, while ASC histopathology was not observed in tumors arising from SPC cells harboring the same genetic mutations (Nagaraj et al., 2017). To investigate the histopathology-selective phenotypes of NSCLC cancer, including potential differences in their transplantation capacity *in vivo*, we first assessed the tumor-forming capacity of bulk cell populations isolated from GEMM-derived KL;ASC and KL;AC cells outside of the lung. $AC^{s.c}$ and $ASC^{s.c.}$ were generated by subcutaneously injecting KL;ASC and KL;AC cells into the flanks of immune compromised athymic nude mice (Fig. 1A). Subcutaneous tumors formed in all nude mice transplanted with KL;AC and KL;ASC cells originally isolated from mixed-colony GEMMs. Tumors derived from KL;ASC transplanted cells ($ASC^{s.c}$) exhibited accelerated growth compared to those derived from KL;AC cells ($AC^{s.c}$) (Fig. 1B), reflected also by a higher relative level of Ki-67 expression in $ASC^{s.c.}$ tumors (Fig. 1C and Fig. S1B). This is consistent with the more aggressive phenotype observed for *in situ* KL;ASC tumors observed in GEMM mice (Nagaraj et al., 2017) and the greater proliferative capacity of GEMM-derived KL;ASC cells that has been previously reported *ex vivo* (Talwelkar et al., 2019). A higher relative growth rate of KL;ASC cells was also detected using primary GEMM-derived cells first established as *ex vivo* cultures prior to s.c. transplantation (Fig. S1A).

Interestingly, immunohistochemical (IHC) end-point analyses revealed that independent of the tumor source (KL;ASC versus KL;AC), resulting s.c. tumors did not exhibit staining for the AC biomarker nkx2-1 (Fig. 1C). $ASC^{s.c.}$ lesions exhibited strong staining for the squamous cell (SCC) marker p63, which was maintained from the source KL;ASC tumor (Fig. 1C), while positive p63 staining in $AC^{s.c.}$ tumors appeared to be associated with stromal cell infiltration rather than a transition to SCC histopathology. Stromal cell infiltration was confirmed with vimentin staining which indeed showed high positivity in both s.c. tumor types (Fig. 1C). Loss of nkx2-1 staining was also observed in $ASC^{s.c.}$ and $AC^{s.c.}$ tumors grown in immune-competent C57BL/6 mice following transplantation of background-matched KL;ASC and KL;AC bulk cell populations (Fig. 1D). Consistent with the immune-compromised mice, these tumors exhibited strong positivity for the mesenchymal marker vimentin, further suggesting stromal cell infiltration. Ki-67 stained positive for a subset of cells suggesting maintenance of proliferative capacity and no differences could be observed between the lesions established in both host strains (Fig. 1D; Fig. S1B). The loss of key histopathological markers and stromal cell infiltration suggests that the subcutaneous transplantation approach does not provide an accurate model to study NSCLC histopathology phenotypes with respect to anti-cancer therapies.

In vivo models where cancer cell lines, including the A549 adenocarcinoma lung cancer cell line, have been intravenously (i.v.) transplanted via mouse tail vein injection have been used to study metastatic processes (Li et al., 2020; Tyagi et al., 2021; Wang et al., 2022; Chen et al., 2021). The contributions of immune cells in modulating lung cancer metastatic processes through i.v. transplantation approaches have however remained limited to the syngeneic squamous Lewis lung cancer model (Qiu et al., 2021), excluding other NSCLC histopathologies. To study the metastatic capability of histopathology-selective NSCLC cells, bulk cell populations from KL;ASC and KL;AC GEMM tumors were i.v. transplanted into athymic nude and C57BL/6 mice (Fig. 2A). In contrast to our observations following s.c. transplantation, only cells from $KL;ASC^{\cdot}$ tumors exhibited the capacity to recolonize the lung, while no tumor formation was observed following i.v. transplantation of KL;AC cells, independent of host immune-competence (Fig. 2B-F). Importantly, the same KL;AC GEMM-derived tumor cells were successfully used for s.c. transplantation (Fig. 1), indicating that while these cells have the capacity to form tumors in recipient mice, they lacked the ability to metastasize to the lungs following i.v. transplantation. Since intravenously injected small cell lung cancer cells have been reported to metastasize livers (Kwon et al., 2015), we analyzed the livers from $ASC^{i.v}$ and $AC^{i.v}$ mice, but observed no tumors [n=5 (ASC), n=4 (AC), results not shown]. $ASC^{i.v}$ tumors were highly aggressive, with host mice requiring sacrifice at a median of 40.4 (nude, n=7) and 25 (C57BL/6, n=15) days post-injection, in comparison to the median latency of KL;ASC GEMMs of 79 days post-tumor initiation (Nagaraj et al., 2017). $ASC^{i.v.}$ tumors were variable in number and size, with a median of nine medium-to-large tumors per lung counted in nude hosts and 19.9 smaller tumors per lung measured in C57BL/6 hosts (Fig. 2B-D; Fig. S2A and B). As cells derived from different KL;ASC GEMM tumors were transplanted into nude versus C57BL/6 recipients, it was not possible to determine if metastasis was accelerated by the intact host immune system of the latter, or a result of tumor heterogeneity.

Biology Open (2022) 11, bio059623. doi:10.1242/bio.059623

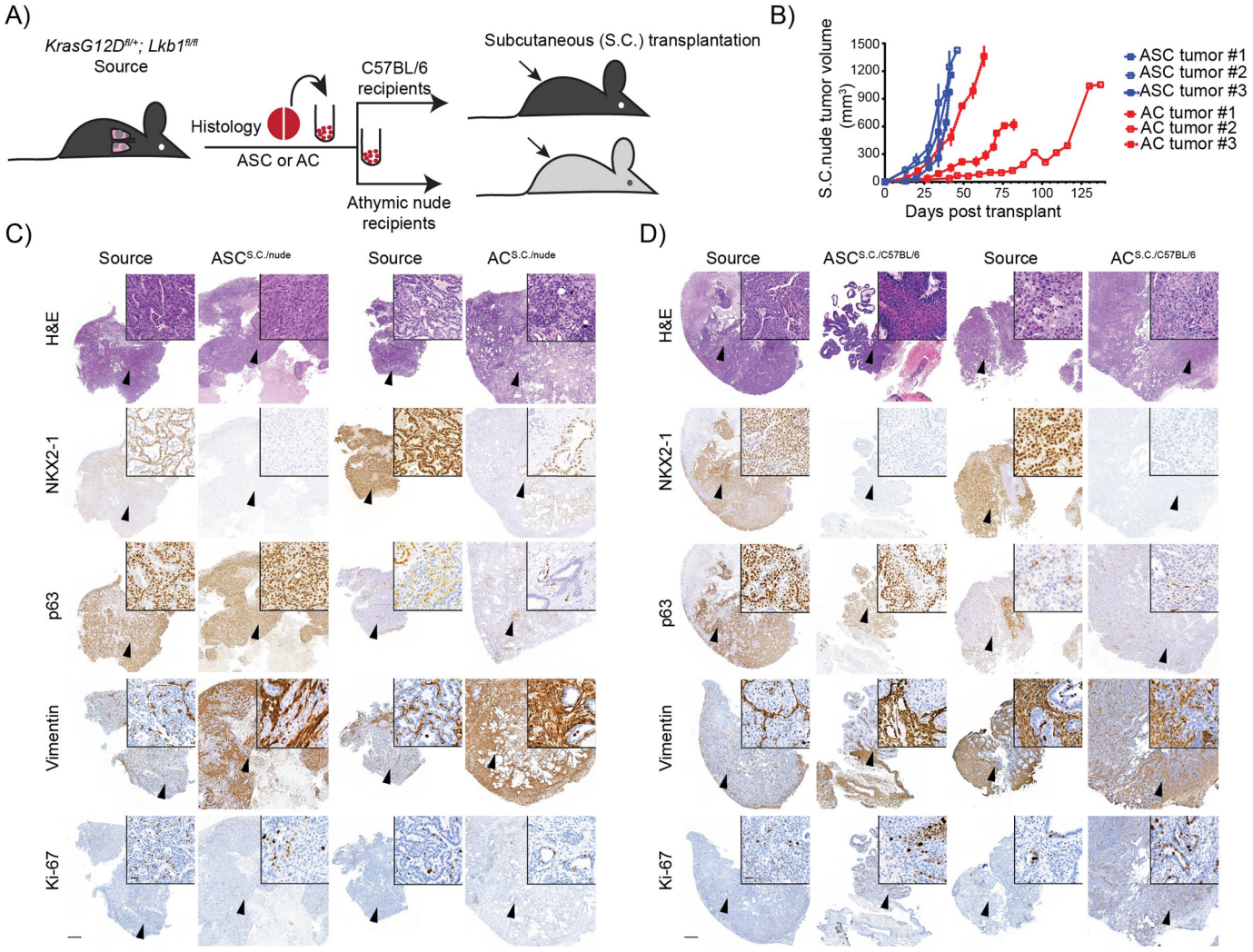

Fig. 1. Host microenvironment-dependent and histopathology-selective tumor establishment subcutaneously. (A) Schematic overview of generation of syngeneic or immune compromised graft models with subcutaneous (s.c.) transplantation of ASC or AC tumor cells derived from KL GEMM mice. Single cell suspensions derived from dissociated KL GEMM source tumors were subjected to dead cell removal prior to transplantation into syngeneic or immune-compromised recipients. A reference tissue piece was fixed from tumors for Haematoxylin and Eosin (H&E) and IHC staining and confirmation of tumor histopathology. (B) Subcutaneous ASC or AC tumor growth curves in athymic nude recipient mice. Each line represents one mouse and the tumors were measured weekly by using a caliper. *n*=3. (C) Representative H&E, nkx2-1/ttf1 and p63 IHC images of source and s.c. tumors from athymic nude recipient mice upon transplantation with ASC or AC tumor-derived cells. Scale bar: 500 µm (2×) or 20 µm (40×). *n*=3. (D) Representative H&E, nkx2-1 and p63 IHC images of source and s.c. tumors from C57BL/6 recipient mice upon transplantation with ASC or AC tumor-derived cells. Scale bar: 500 µm (2×) or 20 µm (40×). *n*=6.

Post-mortal IHC analysis revealed that, again in contrast to results observed in $ASC^{s.c.}$ (Fig. 1C), both AC (nkx2-1) and SCC (p63) characteristics were maintained in $ASC^{i.v.}$ tumors, with the transplanted lesions exhibiting comparable histopathology to the source tumors independent of the host (Fig. 2D and E; Fig. S2A and B). KL tumors have an adaptive activation of receptor tyrosine kinase (RTK) signaling pathways such as the ERBB, MET and MAPK signaling cascades (Manchado et al., 2016). $ASC^{i.v.}$ tumors exhibited positive staining for phosphorylated AKT (pAKT) and ERK1/2 (pERK) that was comparable to the ASC source tumors (Fig. 2E and F; Fig. S3A and B). Consistent with our previous report (Narhi et al., 2018), AC source tumors displayed significantly decreased pAKT levels compared to both $ASC^{i.v.}$ and ASC source tumors, and instead exhibited stronger pERK staining (Fig. S3A and B). While no differences in pEGFR levels could be observed between different mice, for ASC comparable levels of phosphorylated ERBB2 and ERBB3 were observed between source and the transplant-derived tumors, with significantly lower pERBB2 and pERBB3 levels detected in AC source tumors (Fig. S3C-F), which was consistent with our previous observations (Talwelkar et al., 2019). Consequently, in addition to the maintenance of histopathological features, oncogenic signaling pathway activity is maintained in intravenously transplanted ASC lesions compared with source GEMM tumors (Fig. S3C-F).

Maintenance of source tumor-intrinsic and host-systemic immunophenotype of i.v. transplanted ASC lesions

Our previous data indicated a neutrophil-dominating, low T-cell immune phenotype in KL;ASC GEMM tumors (Nagaraj et al., 2017). We therefore assessed whether the immune phenotype of $ASC^{i.v.}$ tumors recapitulated that of the source tumor using IHC analysis of the CD11b neutrophil marker and CD3 T-cell marker. CD3 positivity remained mainly negative throughout $ASC^{i.v}$ tumors in all mice while

Biology Open (2022) 11, bio059623. doi:10.1242/bio.059623

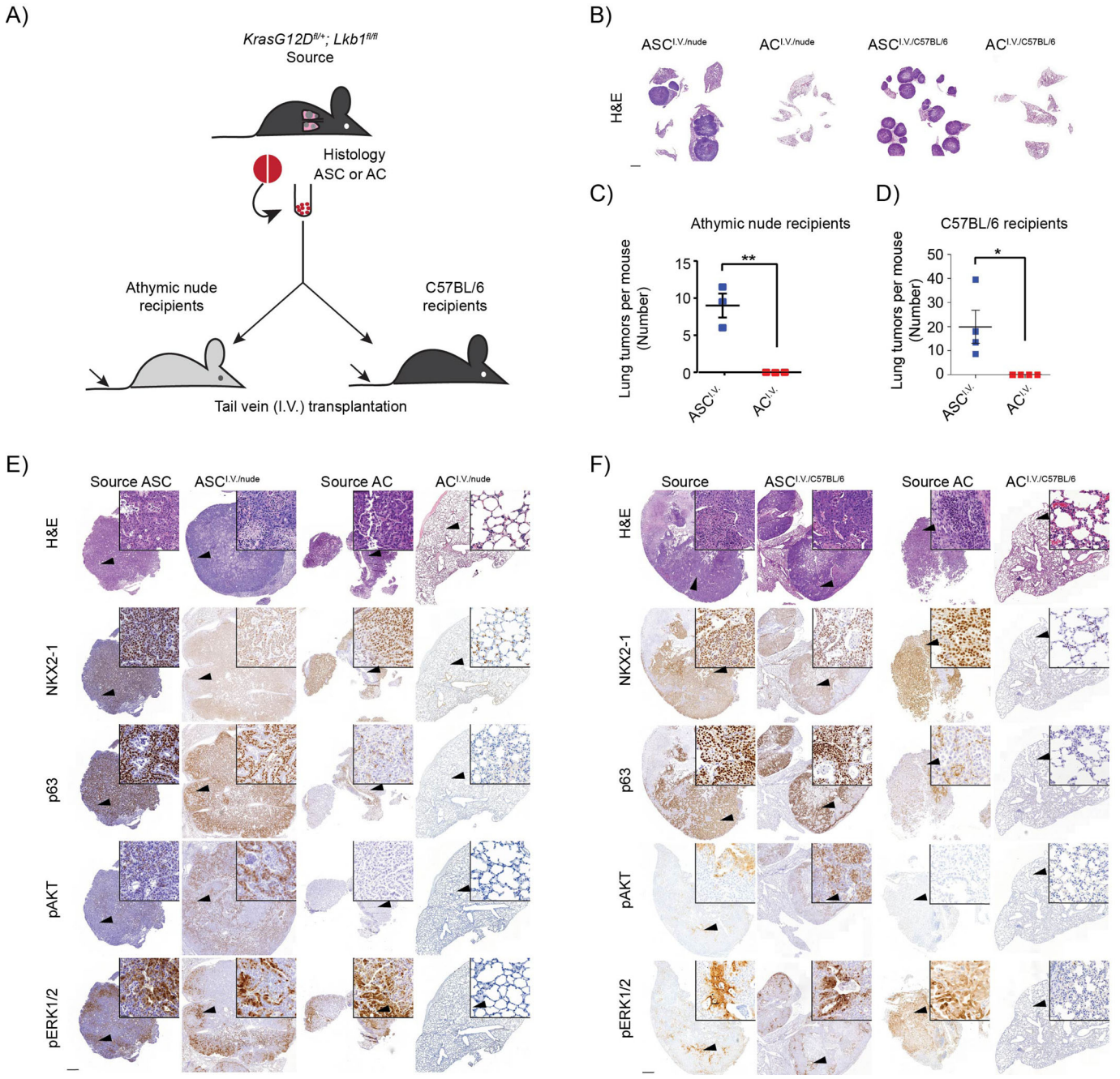

Fig. 2. KL;ASC cells re-colonize to the lung and form tumors after intravenous injection while AC;KL-deficient cells form no tumors. (A) Schematic overview of generation of syngeneic or immune-compromised graft models with intravenous (i.v.) transplantation of ASC or AC transplantation of ASC or AC tumor cells derived from KL GEMM mice. Single cell suspensions derived from dissociated KL GEMM source tumors were subjected to dead cell removal prior to transplantation into syngeneic or immune-compromised recipients. A reference tissue piece was fixed from tumors for H&E and IHC staining and confirmation of tumor histopathology. (B) Representative images of nude and C57BL/6 ASC$^{i.v.}$ and AC$^{i.v.}$ mice whole lungs stained for H&E. Scale bar: 2000 µm (0.4×). *n*=6. (C-D) The number of tumors per mouse was counted based on the H&E stainings performed on tumor tissues. The graph represents mean±s.d. for each group, and each point represents an individual mouse. Two-tailed unpaired Student's *t*-test values are *P<0.05, **P<0.01. *n*=3 (nude); *n*=4 (C57BL/6). (E) Representative H&E, nkx2-1, p63, pAKT and pERK1/2 IHC images of source and i.v. tumors from athymic nude recipient mice upon transplantation with ASC or AC tumor-derived cells. Scale bar: 500 µm (2×) or 20 µm (40×). *n*=3. (F) Representative H&E, nkx2-1, p63, pAKT and pERK1/2 IHC images of source and ASC$^{i.v.}$ tumors from C57BL/6 recipient mice upon transplantation with ASC or AC tumor-derived cells. Scale bar: 500 µm (2×) or 20 µm (40×). *n*=4.

CD11b staining indicative of neutrophil infiltration was more prominent and consistent between ASC$^{i.v}$ lesions and GEMM source tumors (Fig. 3A-B). There were no differences in the percentage of CD11b positive cells between source KL;ASC and ASC$^{i.v.}$ tumors (Fig. S4).

In addition to assessment of tumor-intrinsic immune phenotypes, the relationship between tumor histopathology and the host's systemic immune profile was assessed in the C57BL/6 background. Using flow cytometry CD11b and GR1 positive cells were analyzed in bone marrow, spleen and peripheral blood in both the GEMMs

Biology Open (2022) 11, bio059623. doi:10.1242/bio.059623

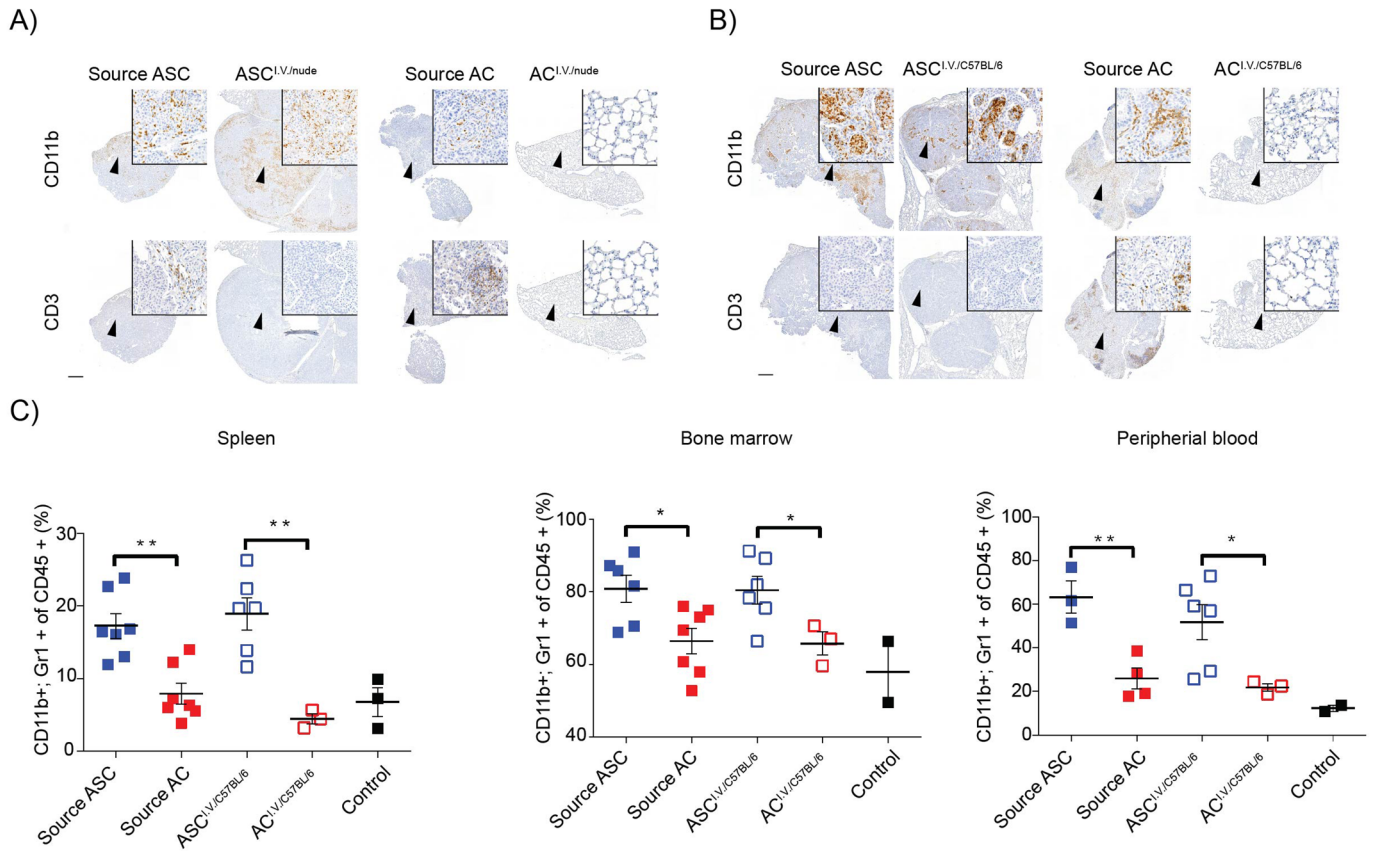

Fig. 3. The immune phenotype in the ASC$^{i.v.}$ model resembles the source ASC immune phenotype. (A) Representative CD11b and CD3 IHC images of source and i.v. tumors from athymic nude recipient mice upon transplantation with ASC or AC tumor-derived cells. Scale bar: 500 µm (2×) or 20 µm (40×). *n*=3. (B) Representative CD11b and CD3 IHC images of source and i.v. tumors from C57BL/6 recipient mice upon transplantation with ASC or AC tumor-derived cells. Scale bar: 500 µm (2×) or 20 µm (40×). *n*=3. (C) Flow cytometric analysis of CD11b+;Gr1+ cells (as a percentage of total CD45+ leukocytes) in bone marrow, peripheral blood and dissociated spleens isolated from ASC-source (Ad5-CC10-Cre infected KL mice), AC-source (Ad5-SPC-Cre infected KL mice) and C57BL/6 recipient mice i.v. transplanted with ASC or AC tumor-derived cells. Controls were C57BL/6 mice that had not been infected with Ad5-Cre or transplanted with tumor cells. Graph represents the mean ±s.e.m. of each group and each point represents an individual mouse. Two-tailed unpaired Student's *t*-test values are **P*<0.05, ***P*<0.01. *n*=3-7.

from which source tumors were originally isolated and the host mice that were subsequently transplanted. GEMMs with KL;ASC tumors had significantly higher levels of CD11b positive cells in all three compartments than GEMMs with KL;AC tumors, which had similar systemic neutrophil populations to non-tumor bearing control mice (Fig. 3C). These results complement previous findings where KL;ASC tumors were reported to have an increased TAN recruitment compared to KL;AC tumors (Nagaraj et al., 2017). Importantly, mice i.v. transplanted with KL;ASC cells (ASC$^{i.v./C57BL/6}$) also exhibited significantly elevated CD11b, GR1 positive cell populations in the spleen, bone marrow and peripheral blood compared to mice transplanted with KL;AC cells (AC$^{i.v./C57BL/6}$) (Fig. 3C). Taken together, the histopathological and immune profiling studies indicate that i.v. transplantation of KL;ASC cells into C57BL/6 hosts (ASC$^{i.v./C57BL/6}$) reliably recapitulates the source GEMM tumor phenotype, rendering it suitable to evaluate anti-cancer treatments for this aggressive subtype of NSCLC.

Therapeutic responses in the ASC$^{i.v.}$ lung transplantation model recapitulate KL;ASC tumors

To investigate how well the i.v. transplantation model mimics NSCLC responses to previously established therapies, we treated ASC$^{i.v./C57BL/6}$ mice with the pan-ERBB inhibitor afatinib (AF). Drug treatments commenced 10 days post-transplantation and continued for four weeks, at which point lung tumor burden was analyzed. Mice in the vehicle control group developed large ASC tumors with 75.5% lung area defined as tumor, while AF-treated mice exhibited significantly lower tumor burden (15.7%; Fig. 4A and B), consistent with previously observed therapeutic response in KL;ASC GEMMs (Talwelkar et al., 2019).

To further explore both the therapeutic response of transplanted tumor cells following lung colonization and the corresponding impact on host survival, ASC$^{i.v./C57BL/6}$, mice were treated with vehicle, AF or the EGFR inhibitor erlotinib (ER) from 10 days post transplantation and sacrificed when they presented with physical signs of disease burden or exhibited 20% body weight loss. All mice, independent of treatment group, developed ASC histotype tumors as indicated by positive nkx2-1 and p63 staining (Fig. S5A). AF, but not ER, treatment provided a significant survival advantage compared to vehicle control (Fig. 4C), suggesting that a selective EGFR inhibitor is insufficient to provide a survival extension in this model. At end-point there was no difference between treatment groups with respect to the proportion of CD11b positive infiltrating neutrophils (Fig. S5B and C), the tumor number per mouse (Fig. S5D) or tumor area in the lungs (Fig. S5E). However, the treatment modulated the KRAS downstream signaling pathway, with significantly decreased staining for phosphorylated ERK1/2, but not

Biology Open (2022) 11, bio059623. doi:10.1242/bio.059623

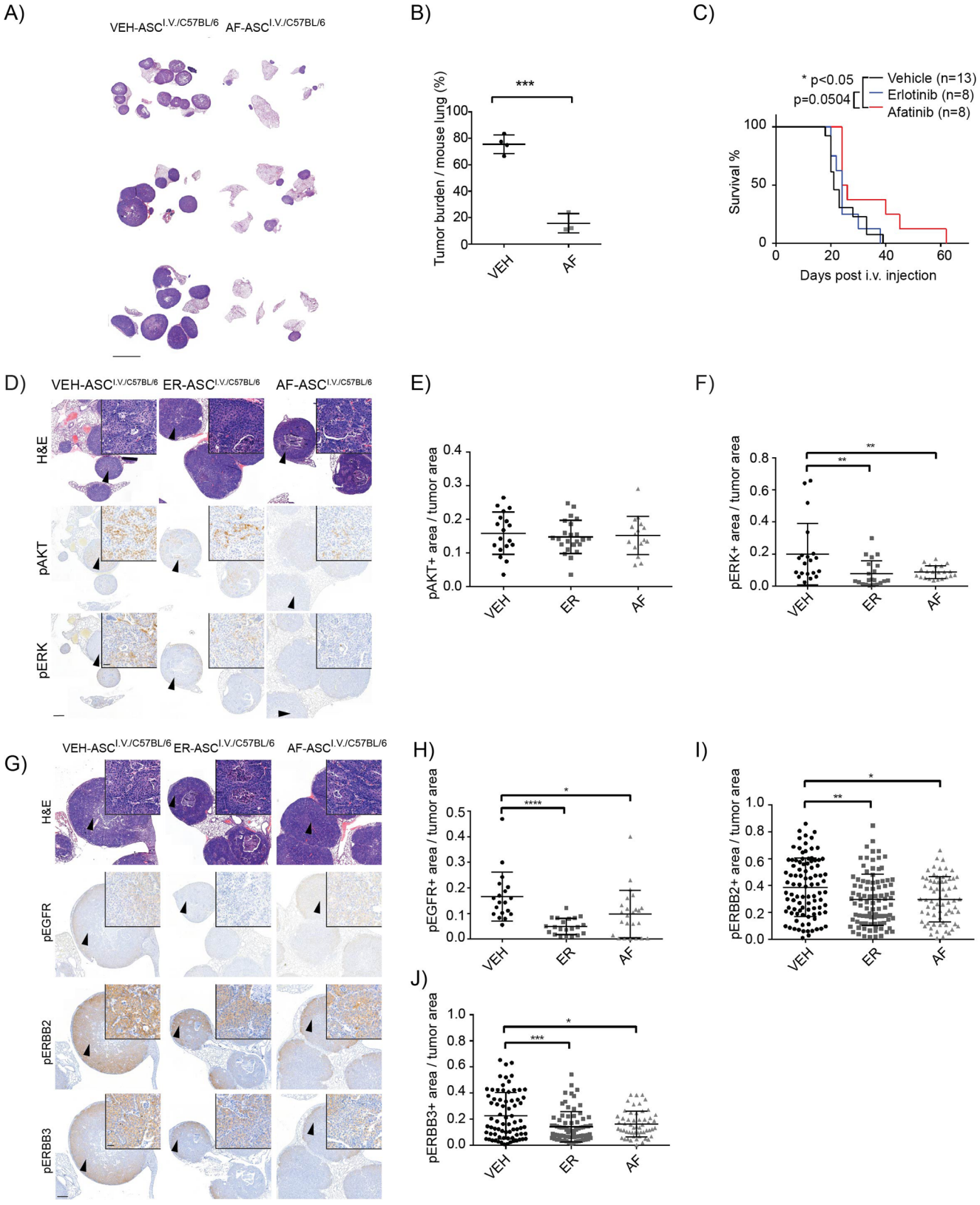

Fig. 4. See next page for legend.

Biology Open (2022) 11, bio059623. doi:10.1242/bio.059623

Fig. 4. ERBB inhibition with afatinib and erlotinib decreases the number of ERBB and pERK positive cells and pan-ERBB inhibition increases the survival of mice. (A) Three representative H&E stainings of mice treated for four weeks 10 days after ASC tumor cell i.v. transplantation with either vehicle control or afatinib (AF). Scale bar: 5000 µm. *n*=4 (VEH); *n*=3 (AF). (B) Quantification of the tumor burden after treatments presented in (A). The graph represents mean ±s.d. for each group, and each point represents an individual mouse. Two-tailed unpaired Student's *t*-test value is ***P<0.001. *n*=4 (VEH); *n*=3 (AF). (C) The survival percentage of mice treated with vehicle, ER and AF 10 days after ASC tumor cell i.v. transplantation. Graph represents the mean ±s.d. for each group, and each point represents an individual mouse. Gehan-Breslow-Wilcoxon test values are *P<0.05. *n*=11 (VEH); *n*=8 (ER/AF). (D) Representative H&E, pAKT and pERK1/2 IHC images of source and i.v. tumors from C57BL/6 recipients upon transplantation with ASC tumor derived cells and treated with vehicle, EGFR inhibitor erlotinib (ER) or pan-ERBB inhibitor afatinib (AF). Scale bar: 500 µm (2×) or 20 µm (40×). *n*=5. (E-F) Quantification of pAKT and pERK1/2 positive area by dividing the positive tumor area with the total tumor area in each tumor separately by using FIJI ImageJ. The graph represents mean ±s.d. for each group, and each point represents an individual tumor. Two-tailed unpaired Student's *t*-test values are **P<0.01. *n*=5. (G) Representative H&E, pEGFR, pERBB2 and pERBB3 IHC images of source and i.v. tumors from C57BL6 recipients upon transplantation with ASC tumor derived cells and treated with vehicle, EGFR inhibitor erlotinib (ER) or pan-ERBB inhibitor afatinib (AF) and euthanized when mice developed health problems. Scale bar: 500 µm (2×) or 20 µm (40×). *n*=5. (H-J) Quantification of pEGFR, pERBB2 and pERBB3 positive area by dividing the positive tumor area with the total tumor area in each tumor separately by using FIJI ImageJ. The graph represents mean ±s.d. for each group, and each point represents an individual tumor. Two-tailed unpaired Student's *t*-test values are *P<0.05, **P<0.01, ***P<0.001. *n*=5.

phosphorylated AKT, detected for both AF and ER treatments (Fig. 4D-F). AF and ER treatment also modified the phosphorylation of key ERBBs including EGFR, ERBB2 and ERBB3, which all exhibited significantly decreased phosphorylation in both AF- and ER-treated mice (Fig. 4G-J). However, for both AF- and ER-treated mice end-point tumors had populations of cells that maintained ERBB phosphorylation, with higher levels maintained in ER-treated mice. This is in line with already published data on KL mice phenotype indicating an improved therapeutic response with pan-ERBB inhibitors compared to EGFR inhibitors (Kruspig et al., 2018; Moll et al., 2018; Talwelkar et al., 2019) further suggesting that our i.v. transplantation model is a reliable preclinical tool for NSCLC therapy and metastasis analysis.

DISCUSSION

There is a need to develop improved, tractable *in vivo* models of NSCLC that accurately reflect the original tumor histopathology, oncogenic signaling profile and immunogenic landscape that can be used to assess therapeutic treatments and potentially provide insights into NSCLC metastatic processes. NSCLC is often diagnosed at a late stage when the disease has already developed metastatic expansions. Even though treatment options for NSCLC have developed enormously during recent years, deeper understanding of NSCLC metastasis is still necessary (Kim et al., 2020). We have here created a reproducible and rapid tumor-lung colonization model to study an aggressive subset of NSCLC via i.v. transplantation of GEMM-derived tumor cells into healthy recipient mice. Importantly the accelerated timeframe of tumor development, with a median survival latency of 25 days in C57BL/6 recipients, was less than half that observed for KL;ASC GEMMs (Nagaraj et al., 2017). Lung-colonizing ASC tumors maintained a histopathology-associated oncogenic signaling phenotype displayed in the source GEMM, and immune-competent C57BL/6 hosts exhibited a previously identified immune-suppressive phenotype characterized by TAN infiltration. Moreover, a systemic immune landscape associated with ASC but not AC NSCLC histopathology, characterized by the expansion of CD11b; Gr1 positive neutrophils in the spleen, bone marrow and bloodstream, was maintained between GEMM and i.v. transplanted mice. The i.v. transplantation model accurately recapitulated ASC sensitivity to the clinically relevant pan-ERBB inhibitor afatinib, through both short-term ablation of localized tumor progression and extended survival upon longer treatment (Moll et al., 2018; Talwelkar et al., 2019).

Despite the equivalent ability of cells derived from GEMM ASC- and AC- lesions to form tumors upon subcutaneous (s.c.) transplantation of both immune-compromised and -competent hosts, lung-colonization upon i.v. transplantation was limited to ASC cells, with AC-injected mice exhibiting no lung tumors or any other indication of disease burden. ASC lesions have been reported to be more aggressive and have a poor prognosis when compared to AC tumors (Nagaraj et al., 2017; Pan et al., 2018), and molecular mechanisms underpinning the differential colonization/ metastatic capacity of tumor cells harboring equivalent genetic driver mutations ($Kras^{G12D/+}$;$Lkb1^{-/-}$) but different histopathology are intriguing. The importance of the squamous cell population, absent in lung-colonized KL;AC populations, for successful tumor formation by transplanted KL;ASC cells is of interest too. The widely used syngeneic Lewis lung cancer model of metastasis following tail vein injection represents squamous histopathology, however there is very limited clinical evidence that squamous NSCLC exhibits greater metastatic potential than adenocarcinoma (Kawase et al., 2012). One of the threshold elements in the metastatic process is the breakage of the extracellular matrix (ECM) and initiation of EMT, which is associated with drug resistance and is typified by the loss of e-cadherin and cell-to-cell connections in favor of increased expression of mesenchymal markers such as expression of vimentin (Peinado et al., 2007; Singh and Settleman, 2010). ASC tumors have been reported to have high levels of chemokine receptors that are associated with increased invasiveness and chemoresistance through insensitivity to apoptotic induction (Zhu et al., 2020). This has been proposed to be dependent upon altered oxidative signaling, and oxidative stress has been reported to inhibit distant metastasis of human melanoma cells in mice (Piskounova et al., 2015). Further studies will be required to determine whether this is a potential route through which ASC cells exhibit superior lung colonization capacity compared to ACs.

In addition to tumor cell phenotypes and genetic drivers, the microenvironment of the tumor plays an important role in both local tumor development as well as metastasis. Interestingly, the maintenance of tumor histopathology was compromised by localized s.c. injection of the ASC and AC cells, with transplant-derived lesions exhibiting stromal infiltration and loss of the AC marker nkx2-1. In contrast, both AC and SCC features were maintained in lung-colonizing tumors formed following ASC i.v. transplantation, pointing to the potential importance of the lung microenvironment for development of key histopathological features. Thus this i.v. lung colonization model serves as a promising tool to investigate the genetic and non-genetic drivers of NSCLC metastases in a histopathology-selective way, and to assess their differential treatment responses.

Adaptive responses driving resistance to targeted drug therapies can potentially be circumvented by combinatorial treatments, such as MEK plus EGFR inhibition. (Kitai et al., 2016). Several reports support the rationale for combination treatment approaches (Kruspig et al., 2018; Manchado et al., 2016), however we have found that

Biology Open (2022) 11, bio059623. doi:10.1242/bio.059623

combinatorial treatment of KL GEMM tumors with afatinib and trametinib did not significantly extend survival beyond single-agent treatments (Talwelkar et al., 2019). Whether this conflicting observation is a consequence of intra- and inter-mouse tumor heterogeneity in the KL GEMMs that is absent in cell-line based xenograft therapy studies is an open question. Thus, we sought to determine if our GEMM-derived lung colonization model could serve as an alternative tool to model *KRAS*-mutant NSCLC responses to novel therapeutic strategies. The i.v. ASC transplantation model robustly recapitulated our previously reported results using KL GEMMs and *ex vivo* culture systems. AF single treatment ablated tumor growth in the lungs upon short-term treatment and significantly prolonged survival following extended therapy, a benefit not provided by single-agent ER treatment which is consistent with earlier studies (Kruspig et al., 2018; Moll et al., 2018). Profiling of phosphorylated ERBB2 and ERBB3 in end-stage tumors indicated that on-target activity of AF was sustained despite tumor progression, pointing to the emergence of alternative resistance mechanisms that could in the future be explored further. Investigating the i.v. transplanted ASC tumor cells with lineage tracing methods could provide answers on what adaptive signaling pathways are activated upon treatments, and if combinatorial therapy could provide an increased efficacy.

In addition to agents targeting key NSCLC oncogenic pathways, our lung colonization model provides opportunities to assess other therapeutic strategies including immune-focused approaches. Neutrophils often predominate the immune landscape in NSCLC microenvironments and can limit the efficacy of immune-checkpoint blockade treatment options such as anti-PD-L1 therapy (Rapoport et al., 2020). We and others have previously reported neutrophil infiltration and low T-cell abundance in $Kras^{G12D/+}$;$Lkb1^{-/-}$ and $Lkb^{-/-}$ tumors, which was recapitulated in our $ASC^{i.v.}$ lung colonization model (Koyama et al., 2016; Nagaraj et al., 2017). We have here also reported ASC-specific systemic neutrophil expansion in KL GEMMs that is also present in i.v. ASC transplanted mice. Underpinning their promise as therapeutic targets, neutrophils have specifically been reported to support the initiation of cancer cell metastasis in solid tumors (Xing et al., 2021; Guan et al., 2021; Wculek and Malanchi, 2015; Tohme et al., 2016; Schneider et al., 2021). Strategies that impair neutrophil functions may therefore serve as an approach to inhibit metastatic progression, with selective promise for ASC histotype NSCLC. A consequence of neutrophil expansion during inflammation is the formation of stress-associated neutrophil extracellular traps (NET), which have also been shown to regulate both tumor initiation and metastatic processes (Masucci et al., 2020). A strategy to inhibit colorectal cancer growth and metastasis has been to target NETs either directly by local DNase treatment or by inhibition of peptidylarginine deaminase, which is essential for NET formation (Tohme et al., 2016). Another option for targeting neutrophils could be to target chemokines, such as TGF-β1, that have been shown to stimulate the tumor-infiltration by neutrophils (Jayaraman et al., 2018).

In summary, we present a tractable approach to faithfully model NSCLC in a setting that will provide options to investigate metastatic capacities of cells and molecular profiles that dictate responses to targeted therapies. We highlight the unique capacity of KL;ASC, but not KL;AC, tumor cells to effectively re-colonize the lung in recipient i.v. transplanted mice, with histopathological features, oncogenic signaling profiles and previously characterized therapeutic responses maintained. We also show that the TME plays a crucial role in the development of tumors with uniform loss of a benchmark AC molecular marker in subcutaneous tumors independent of the source GEMM lesions. In conclusion, we put forward our lung colonization model as a robust tool to identify improved treatment approaches for NSCLC and solutions to enable the prevention and control of NSCLC tumor metastasis.

MATERIALS AND METHODS

Animal models and tumor initiation in NSCLC GEMMs

All aspects of animal handling and studies were performed by following the guidelines from the Finnish National Board of Animal Experimentation (permit number ESAVI/6365/2019). $Kras^{LSL(G12D)/WT}$ mice (Jackson et al., 2001) were purchased from The Jackson Laboratory. $Lkb1^{fl/fl}$ mice (Bardeesy et al., 2002) were received from Ronald DePinho (MD Anderson). $Kras^{LSL(G12D)/WT}$ (C57BL/6J background) were bred with $Lkb1^{fl/fl}$ (F4 ICR;BALB/cByJ;FVB/N background) to generate $Kras^{LSL(G12D)/WT}$;$Lkb1^{fl/fl}$ (KL) strains (Ji et al., 2007). 3-week-old Hsd:AthymicNude-Foxn1nu were purchased from ENVIGO (Huntingdon). To initiate tumor formation, 8–12-week-old KL mice (mixed background and C57BL/6 pure background) were intranasally infected with 10^7 plaque forming units (PFU) AD5-CC10-Cre or 10^9 PFU Ad5-SPC-Cre (Viral Vector Core Facility, University of Iowa) per mouse in 60 micro (litre) total volume of medium (MEM, Sigma-Aldrich) with 9.67 mM $CaCl_2$. Mice were sacrificed by cervical dislocation or CO_2 inhalation upon presentation with labored breathing and weight loss. Both female and male mice were used in similar numbers in all experiments.

Generation of intravenous and subcutaneous transplantation models

Mixed background and C57BL/6 *KL* mice were infected with Ad5-CC10-Cre or Ad5-SPC-Cre and were sacrificed upon presentation with labored breathing and weight loss, with median survival of 105 (ASC-bearing mice) and 116 days (AC-bearing mice) post-infection observed. Lungs with tumors were dissected and placed in HBSS. Tumors were isolated from lungs and a tissue reference piece was separated and fixed in 4% paraformaldehyde (Merck) overnight at 4°C. Single cell suspensions were generated from remaining tumor tissue in a digestion mixture with 2 mg/ml Collagenase and 0.3 mg/ml Dispase in HBSS for 30 min in 37°C. Tissue pieces were thereafter mechanically disrupted with gentle MACS tube (Miltenyi Biotec) in cold DMEM with 10% heat-inactivated fetal bovine serum (HI-FBS), 1% Glutamine and 5 µl/ml DNase using the gentle MACS dissociator. The cells were filtered with a 70 µm cell strainer and dead cell removal was performed on single cell suspensions (Miltenyi Biotec) and live tumor cells were frozen in 90% HI-FBS and 10% dimethyl sulfoxide (DMSO). Live tumor cells were revived, washed once with phosphate buffered saline (PBS) and re-suspended in PBS at a concentration of 2×10^5 cells/100 µl (for i.v. injection) or $6.6–10\times10^5$ cells/100 µl (for s.c. injection). Single cell suspensions were injected i.v. (tail vein) or s.c. (right flank) into recipient 4–8-week-old Hsd:AthymicNude-Foxn1nu or C57BL/6 mice with a 30 gauge needle. I.v.-injected mice were sacrificed upon presentation with labored breathing and weight loss or reaching 10 weeks post-transplantation. Lungs with tumors were washed with HBSS and fixed in 4% paraformaldehyde overnight at 4°C. Blood was isolated from the saphenous vein immediately following sacrifice, collected into tubes containing 10 mM EDTA. Spleens were dissected and bone marrow was flushed from femurs and tibias with a 26 gauge needle. Spleens were mechanically dissociated (gentleMACS™) white blood cells were isolated from whole blood, bone marrow and spleens by performing red blood cell lysis. White blood cells suspensions from whole blood, spleens and bone marrow were stained with fluorophore-conjugated antibodies for 30 min at 4°C and cells were analyzed by flow cytometry (Intellicyt iQUE PLUS screener and Forecyt analysis software). See Table S1 for a list of conjugated antibodies and concentrations. Tumor growth in s.c. injected mice were monitored by manual caliper measurements and mice were sacrificed upon (i) s.c. tumor reaching 1300 mm^3; (ii) exhibition of inflammation or irritation at tumor site or; (iii) reaching 6 months post-injection. Upon sacrifice, s.c. tumors were dissected, washed with HBSS, cut into multiple pieces and fixed in 4% paraformaldehyde overnight at 4°C.

In vivo treatment with afatinib and erlotinib

ASC tumor cells were transplanted into age-matched C57BL/6 mice in order to generate tumors. Treatment with afatinib (12.5 mg/kg; MedChemExpress) or erlotinib (12.5 mg/kg; MedChemExpress) in 0.5% hydroxyl propyl methyl cellulose and 0.1% Tween 80 in H_2O by oral gavage was started 10 days after tumor cell injection. For the analysis of tumor burden at 4 weeks after injection (Fig. 4A-B), mice were treated with afatinib 3 days per week. In the survival analysis, mice were treated five times per week and euthanized when their weight dropped more than 20% or their health weakened. Mice were euthanized by cervical dislocation and tumors were collected for IHC analysis.

IHC and histopathology analysis

Formalin fixed tissues were dehydrated in absolute ethanol and isopropanol and embedded in paraffin (FFPE). 4 µm sections were cut and dried overnight at 37°C. FFPE sections were rehydrated, and stained with H&E (Merck and Sigma-Aldrich) or IHC using antibodies of interest. Rehydrated tissue sections underwent heat-mediated antigen-epitope retrieval in 10 mM citric acid buffer pH6 or 10 mM Tris/ 1 mM EDTA buffer pH9 (Lab Vision^{TM} PT Module, Thermo Fisher Scientific), endogenous peroxidase blocking with 0.3% H_2O_2 (31642, Sigma-Aldrich) for 30 min at room temperature and non-specific blocking with 1% bovine serum albumin (BSA; A2153, Sigma-Aldrich) and 10% normal goat serum (NGS; Gibco) for 30 min at room temperature. Primary antibodies were diluted in 5% NGS and tissue sections were incubated with primary antibodies for 1-2 h at room temperature. BrightVision poly-HRP Goat anti-Rabbit (ImmunoLogic) was used as the secondary antibody and substrate detection was performed with DAB (Bright DAB, ImmunoLogic). Counterstaining was performed with 10% Haematoxylin (Dako) and after dehydration slides were mounted with DPX mounting medium (Merck). Whole slide scans of H&E and IHC-stained lung and tumor sections were acquired with a Pannoramic 250 digital slide scanner using a 20× objective (3DHISTECH, Budapest, Hungary). Images of whole slide scans and snapshots were acquired using the online WebMicroscope platform (fimm.webmicroscope.net). See Table S1 for a list of IHC antibodies and concentrations.

Transplantation of *ex vivo* conditionally reprogrammed culture

Conditionally reprogrammed cultures (CRCs) of ASC and AC tumors isolated from KL;CC10 and KL;SPC mice were previously generated and were maintained in co-culture with γ-irradiated NIH3T3 fibroblasts in F12/DMEM media supplemented with 5% HI-FBS, 5 mg/ml insulin (I2643, Sigma-Aldrich), 24 mg/ml adenine (A2786, Sigma-Aldrich), 10 mM Y-27632 (ALX-270-M0055, Enzo Life Sciences), 10 ng/ml human recombinant epidermal growth factor (hr-EGF; 354052, BD Pharmigen), 0.4 mg/ml hydrocortisone (Sigma-Aldrich), 10 ng/ml cholera toxin (1000B, List Biological Laboratories) and 1% penicillin/streptomycin (15140122, Thermo Fisher Scientific). 5-10×10^5 CRC cells were subcutaneously injected to the flanks of nude mice and the tumors were measured weekly with a caliper.

Statistical analysis

Gehan–Breslow–Wilcoxon test was used for the mouse survival curve analysis. One-way analysis of variance (ANOVA) tests with Tukey's multiple comparisons tests were used to test statistical significance in the mouse IHC-based quantifications. For all other analyses, Student's two-tailed *t*-test and equal variance were used with the following *P*-values: **P*<0.05, ***P*<0.01, ****P*<0.001. All experiments were repeated at least three times on different days.

Acknowledgements

We are grateful to Tomi Mäkelä and Ronald DePinho for the *Lkb$^{fl/fl}$* mice. We thank the FIMM digital microscopy unit for scanning histological slides, and the HiLIFE Laboratory Animal Centre Core Facility at the University of Helsinki for animal husbandry care and support. We thank Kaisa Salmenkivi and Mikko Mäyränpää for histopathology consultation. We thank past and present members of the Verschuren lab for guidance and support.

Competing interests

The authors declare no competing or financial interests.

Author contributions

Conceptualization: J.R.D., E.W.V.; Methodology: I.A.K.L., J.R.D., S.S.T., N.L., C.S., E.A.K., A.H.; Validation: I.A.K.L., J.R.D., A.S.N., S.S.T., E.W.V.; Formal analysis: I.A.K.L., J.R.D., A.S.N.; Investigation: I.A.K.L., J.R.D., A.S.N., S.S.T., J.B., N.L., C.S., A.H., E.W.V.; Resources: J.R.D., A.S.N., E.W.V.; Data curation: S.S.T.; Writing - original draft: I.A.K.L., J.R.D., E.W.V.; Writing - review & editing: I.A.K.L., J.R.D., E.W.V.; Visualization: I.A.K.L., J.R.D., A.S.N., J.B., N.L., C.S., A.H.; Supervision: E.W.V.; Project administration: I.A.K.L., J.R.D., E.W.V.; Funding acquisition: I.A.K.L., E.W.V.

Funding

Research was supported by the Liv och Hälsa foundation (E.W.V., I.A.K.L.), the University of Helsinki Doctoral Programme in Biomedicine (A.S.N, J.B.), the University of Helsinki Integrative Life Science doctoral program (S.S.T.); the Academy of Finland (E.W.V. grant 307111), and the Finnish Cancer Organizations (E.W.V. grant 4706132). Open Access funded by Helsinki University Library.

Data availability

All relevant data can be found within the article and its supplementary information.

References

Bardeesy, N., Sinha, M., Hezel, A. F., Signoretti, S., Hathaway, N. A., Sharpless, N. E., Loda, M., Carrasco, D. R. and Depinho, R. A. (2002). Loss of the Lkb1 tumour suppressor provokes intestinal polyposis but resistance to transformation. *Nature* **419**, 162-167. doi:10.1038/nature01045

Brahmer, J., Reckamp, K. L., Baas, P., Crino, L., Eberhardt, W. E., Poddubskaya, E., Antonia, S., Pluzanski, A., Vokes, E. E., Holgado, E. et al. (2015). Nivolumab versus Docetaxel in advanced squamous-cell non-small-cell lung cancer. *N. Engl. J. Med.* **373**, 123-135. doi:10.1056/NEJMoa1504627

Bray, F., Ferlay, J., Soerjomataram, I., Siegel, R. L., Torre, L. A. and Jemal, A. (2018). Global cancer statistics 2018: GLOBOCAN estimates of incidence and mortality worldwide for 36 cancers in 185 countries. *CA Cancer J. Clin.* **68**, 394-424. doi:10.3322/caac.21492

Calles, A., Liao, X., Sholl, L. M., Rodig, S. J., Freeman, G. J., Butaney, M., Lydon, C., Dahlberg, S. E., Hodi, F. S., Oxnard, G. R. et al. (2015). Expression of PD-1 and its ligands, PD-L1 and PD-L2, in smokers and never smokers with KRAS-mutant lung cancer. *J. Thorac. Oncol.* **10**, 1726-1735. doi:10.1097/JTO.0000000000000687

Chaffer, C. L. and Weinberg, R. A. (2011). A perspective on cancer cell metastasis. *Science* **331**, 1559-1564. doi:10.1126/science.1203543

Chen, T., Li, D., Feng, C., Zhang, Z., Zhu, D., Li, D. and Zhao, X. (2021). Huaier increases the antitumor effect of gemcitabine on pancreatic cancer in vitro and in vivo. *Transl. Cancer Res.* **10**, 1368-1377. doi:10.21037/tcr-20-2627

Gettinger, S. N., Horn, L., Gandhi, L., Spigel, D. R., Antonia, S. J., Rizvi, N. A., Powderly, J. D., Heist, R. S., Carvajal, R. D., Jackman, D. M. et al. (2015). Overall survival and long-term safety of nivolumab (anti-programmed death 1 antibody, BMS-936558, ONO-4538) in patients with previously treated advanced non-small-cell lung cancer. *J. Clin. Oncol.* **33**, 2004-2012. doi:10.1200/JCO.2014.58.3708

Guan, X., Lu, Y., Zhu, H., Yu, S., Zhao, W., Chi, X., Xie, C. and Yin, Z. (2021). The crosstalk between cancer cells and neutrophils enhances hepatocellular carcinoma metastasis via neutrophil extracellular traps-associated Cathepsin G component: a potential therapeutic target. *J. Hepatocell Carcinoma.* **8**, 451-465. doi:10.2147/JHC.S303588

Jackson, E. L., Willis, N., Mercer, K., Bronson, R. T., Crowley, D., Montoya, R., Jacks, T. and Tuveson, D. A. (2001). Analysis of lung tumor initiation and progression using conditional expression of oncogenic K-ras. *Genes Dev.* **15**, 3243-3248. doi:10.1101/gad.943001

Jayaraman, P., Parikh, F., Newton, J. M., Hanoteau, A., Rivas, C., Krupar, R., Rajapakshe, K., Pathak, R., Kanthaswamy, K., Maclaren, C. et al. (2018). TGF-beta1 programmed myeloid-derived suppressor cells (MDSC) acquire immune-stimulating and tumor killing activity capable of rejecting established tumors in combination with radiotherapy. *Oncoimmunology* **7**, e1490853. doi:10.1080/2162402X.2018.1490853

Ji, H., Ramsey, M. R., Hayes, D. N., Fan, C., Mcnamara, K., Kozlowski, P., Torrice, C., Wu, M. C., Shimamura, T., Perera, S. A. et al. (2007). LKB1 modulates lung cancer differentiation and metastasis. *Nature* **448**, 807-810. doi:10.1038/nature06030

Kawase, A., Yoshida, J., Ishii, G., Nakao, M., Aokage, K., Hishida, T., Nishimura, M. and Nagai, K. (2012). Differences between squamous cell carcinoma and adenocarcinoma of the lung: are adenocarcinoma and squamous cell carcinoma prognostically equal? *Jpn. J. Clin. Oncol.* **42**, 189-195. doi:10.1093/jjco/hyr188

Kim, M., Mun, H., Sung, C. O., Cho, E. J., Jeon, H. J., Chun, S. M., Jung, D. J., Shin, T. H., Jeong, G. S., Kim, D. K. et al. (2019). Patient-derived lung cancer

organoids as in vitro cancer models for therapeutic screening. *Nat. Commun.* **10**, 3991. doi:10.1038/s41467-019-11867-6

Kim, D., Xue, J. Y. and Lito, P. (2020). Targeting KRAS(G12C): from inhibitory mechanism to modulation of antitumor effects in patients. *Cell* **183**, 850-859. doi:10.1016/j.cell.2020.09.044

Kitai, H., Ebi, H., Tomida, S., Floros, K. V., Kotani, H., Adachi, Y., Oizumi, S., Nishimura, M., Faber, A. C. and Yano, S. (2016). Epithelial-to-mesenchymal transition defines feedback activation of receptor tyrosine kinase signaling induced by MEK inhibition in KRAS-mutant lung cancer. *Cancer Discov.* **6**, 754-769. doi:10.1158/2159-8290.CD-15-1377

Koyama, S., Akbay, E. A., Li, Y. Y., Aref, A. R., Skoulidis, F., Herter-Sprie, G. S., Buczkowski, K. A., Liu, Y., Awad, M. M., Denning, W. L. et al. (2016). STK11/LKB1 deficiency promotes neutrophil recruitment and proinflammatory cytokine production to suppress T-cell activity in the lung tumor microenvironment. *Cancer Res.* **76**, 999-1008. doi:10.1158/0008-5472.CAN-15-1439

Kruspig, B., Monteverde, T., Neidler, S., Hock, A., Kerr, E., Nixon, C., Clark, W., Hedley, A., Laing, S., Coffelt, S. B. et al. (2018). The ERBB network facilitates KRAS-driven lung tumorigenesis. *Sci. Transl. Med.* **10**, eaao2565. doi:10.1126/scitranslmed.aao2565

Kwon, M. C., Proost, N., Song, J. Y., Sutherland, K. D., Zevenhoven, J. and Berns, A. (2015). Paracrine signaling between tumor subclones of mouse SCLC: a critical role of ETS transcription factor Pea3 in facilitating metastasis. *Genes Dev.* **29**, 1587-1592. doi:10.1101/gad.262998.115

Li, P., Lu, M., Shi, J., Hua, L., Gong, Z., Li, Q., Shultz, L. D. and Ren, G. (2020). Dual roles of neutrophils in metastatic colonization are governed by the host NK cell status. *Nat. Commun.* **11**, 4387. doi:10.1038/s41467-020-18125-0

Li, Y., Hu, L., Peng, X., Xu, H., Tang, B. and Xu, C. (2022). Resistance to immune checkpoint inhibitors in KRAS-mutant non-small cell lung cancer. *Cancer Drug Resist.* **5**, 129-146. doi:10.20517/cdr.2021.102

Liu, X., Ory, V., Chapman, S., Yuan, H., Albanese, C., Kallakury, B., Timofeeva, O. A., Nealon, C., Dakic, A., Simic, V. et al. (2012). ROCK inhibitor and feeder cells induce the conditional reprogramming of epithelial cells. *Am. J. Pathol.* **180**, 599-607. doi:10.1016/j.ajpath.2011.10.036

Liu, B., Liu, H., Ma, Y., Ding, Q., Zhang, M., Liu, X. and Liu, M. (2021). EGFR-mutated stage IV non-small cell lung cancer: what is the role of radiotherapy combined with TKI? *Cancer Med.* **10**, 6167-6188. doi:10.1002/cam4.4192

Manchado, E., Weissmueller, S., Morris, J. P., Chen, C. C., Wullenkord, R., Lujambio, A., De Stanchina, E., Poirier, J. T., Gainor, J. F., Corcoran, R. B. et al. (2016). A combinatorial strategy for treating KRAS-mutant lung cancer. *Nature* **534**, 647-651. doi:10.1038/nature18600

Masucci, M. T., Minopoli, M., Del Vecchio, S. and Carriero, M. V. (2020). The emerging role of neutrophil extracellular traps (NETs) in tumor progression and metastasis. *Front. Immunol.* **11**, 1749. doi:10.3389/fimmu.2020.01749

Moll, H. P., Pranz, K., Musteanu, M., Grabner, B., Hruschka, N., Mohrherr, J., Aigner, P., Stiedl, P., Brcic, L., Laszlo, V. et al. (2018). Afatinib restrains K-RAS-driven lung tumorigenesis. *Sci. Transl. Med.* **10**, eaao2301. doi:10.1126/scitranslmed.aao2301

Nagaraj, A. S., Lahtela, J., Hemmes, A., Pellinen, T., Blom, S., Devlin, J. R., Salmenkivi, K., Kallioniemi, O., Mayranpaa, M. I., Narhi, K. et al. (2017). Cell of origin links histotype spectrum to immune microenvironment diversity in non-small-cell lung cancer driven by mutant Kras and loss of Lkb1. *Cell Rep.* **18**, 673-684. doi:10.1016/j.celrep.2016.12.059

Narhi, K., Nagaraj, A. S., Parri, E., Turkki, R., Van Duijn, P. W., Hemmes, A., Lahtela, J., Uotinen, V., Mayranpaa, M. I., Salmenkivi, K. et al. (2018). Spatial aspects of oncogenic signalling determine the response to combination therapy in slice explants from Kras-driven lung tumours. *J. Pathol.* **245**, 101-113. doi:10.1002/path.5059

Pan, F., Cui, S., Wang, W., Gu, A. and Jiang, L. (2018). Survival analysis for lung adenosquamous carcinoma patients with brain metastasis. *J. Cancer* **9**, 3707-3712. doi:10.7150/jca.27441

Peinado, H., Olmeda, D. and Cano, A. (2007). Snail, Zeb and bHLH factors in tumour progression: an alliance against the epithelial phenotype? *Nat. Rev. Cancer* **7**, 415-428. doi:10.1038/nrc2131

Piskounova, E., Agathocleous, M., Murphy, M. M., Hu, Z., Huddlestun, S. E., Zhao, Z., Leitch, A. M., Johnson, T. M., Deberardinis, R. J. and Morrison, S. J. (2015). Oxidative stress inhibits distant metastasis by human melanoma cells. *Nature* **527**, 186-191. doi:10.1038/nature15726

Qiu, W.-L., Hsu, W.-H., Tsao, S.-M., Tseng, A.-J., Lin, Z.-H., Hua, W.-J., Yeh, H., Lin, T.-E., Chen, C.–C., Chen, L.-S. et al. (2021). WSG, a glucose-rich polysaccharide from ganoderma lucidum, combined with cisplatin potentiates inhibition of lung cancer in vitro and in vivo. *Polymers* **13**, 4353. doi:10.3390/polym13244353

Quinn, J. J., Jones, M. G., Okimoto, R. A., Nanjo, S., Chan, M. M., Yosef, N., Bivona, T. G. and Weissman, J. S. (2021). Single-cell lineages reveal the rates, routes, and drivers of metastasis in cancer xenografts. *Science* **371**, eabc1944. doi:10.1126/science.abc1944

Rapoport, B. L., Steel, H. C., Theron, A. J., Smit, T. and Anderson, R. (2020). Role of the neutrophil in the pathogenesis of advanced cancer and impaired responsiveness to therapy. *Molecules* **25**, 1618. doi:10.3390/molecules25071618

Sachs, N., Papaspyropoulos, A., Zomer-Van Ommen, D. D., Heo, I., Bottinger, L., Klay, D., Weeber, F., Huelsz-Prince, G., Iakobachvili, N., Amatngalim, G. D. et al. (2019). Long-term expanding human airway organoids for disease modeling. *EMBO J.* **38**, e100300. doi:10.15252/embj.2018100300

Schabath, M. B., Welsh, E. A., Fulp, W. J., Chen, L., Teer, J. K., Thompson, Z. J., Engel, B. E., Xie, M., Berglund, A. E., Creelan, B. C. et al. (2016). Differential association of STK11 and TP53 with KRAS mutation-associated gene expression, proliferation and immune surveillance in lung adenocarcinoma. *Oncogene* **35**, 3209-3216. doi:10.1038/onc.2015.375

Schneider, M., Schafer, N., Bode, C., Borger, V., Eichhorn, L., Giordano, F. A., Guresir, E., Heimann, M., Ko, Y. D., Lehmann, F. et al. (2021). Prognostic value of preoperative inflammatory markers in melanoma patients with brain metastases. *J. Clin. Med.* **10**, 634. doi:10.3390/jcm10040634

Singh, A. and Settleman, J. (2010). EMT, cancer stem cells and drug resistance: an emerging axis of evil in the war on cancer. *Oncogene* **29**, 4741-4751. doi:10.1038/onc.2010.215

Skoulidis, F., Byers, L. A., Diao, L., Papadimitrakopoulou, V. A., Tong, P., Izzo, J., Behrens, C., Kadara, H., Parra, E. R., Canales, J. R. et al. (2015). Co-occurring genomic alterations define major subsets of KRAS-mutant lung adenocarcinoma with distinct biology, immune profiles, and therapeutic vulnerabilities. *Cancer Discov.* **5**, 860-877. doi:10.1158/2159-8290.CD-14-1236

Skoulidis, F., Goldberg, M. E., Greenawalt, D. M., Hellmann, M. D., Awad, M. M., Gainor, J. F., Schrock, A. B., Hartmaier, R. J., Trabucco, S. E., Gay, L. et al. (2018). STK11/LKB1 mutations and PD-1 inhibitor resistance in KRAS-mutant lung adenocarcinoma. *Cancer Discov.* **8**, 822-835. doi:10.1158/2159-8290.CD-18-0099

Talwelkar, S. S., Nagaraj, A. S., Devlin, J. R., Hemmes, A., Potdar, S., Kiss, E. A., Saharinen, P., Salmenkivi, K., Mayranpaa, M. I., Wennerberg, K. et al. (2019). Receptor tyrosine kinase signaling networks define sensitivity to ERBB inhibition and stratify Kras-mutant lung cancers. *Mol. Cancer Ther.* **18**, 1863-1874. doi:10.1158/1535-7163.MCT-18-0573

Talwelkar, S. S., Mayranpaa, M. I., Soraas, L., Potdar, S., Bao, J., Hemmes, A., Linnavirta, N., Lomo, J., Rasanen, J., Knuuttila, A. et al. (2021). Functional diagnostics using fresh uncultured lung tumor cells to guide personalized treatments. *Cell Rep. Med.* **2**, 100373. doi:10.1016/j.xcrm.2021.100373

Tohme, S., Yazdani, H. O., Al-Khafaji, A. B., Chidi, A. P., Loughran, P., Mowen, K., Wang, Y., Simmons, R. L., Huang, H. and Tsung, A. (2016). Neutrophil extracellular traps promote the development and progression of liver metastases after surgical stress. *Cancer Res.* **76**, 1367-1380. doi:10.1158/0008-5472.CAN-15-1591

Tyagi, A., Sharma, S., Wu, K., Wu, S. Y., Xing, F., Liu, Y., Zhao, D., Deshpande, R. P., D'Agostino, R. B., Jr. and Watabe, K. (2021). Nicotine promotes breast cancer metastasis by stimulating N2 neutrophils and generating pre-metastatic niche in lung. *Nat. Commun.* **12**, 474. doi:10.1038/s41467-020-20733-9

Wang, R., Chen, J., Yu, H., Wei, Z., Ma, M., Ye, X., Wu, W., Chen, H. and Fu, Z. (2022). Downregulation of estrogen receptor-alpha36 expression attenuates metastasis of hepatocellular carcinoma cells. *Environ. Toxicol.* **37**, 1113-1123. doi:10.1002/tox.23469

Wculek, S. K. and Malanchi, I. (2015). Neutrophils support lung colonization of metastasis-initiating breast cancer cells. *Nature* **528**, 413-417. doi:10.1038/nature16140

Xing, X., Bai, Y. and Song, J. (2021). The heterogeneity of neutrophil recruitment in the tumor microenvironment and the formation of premetastatic Niches. *J. Immunol. Res.* **2021**, 6687474. doi:10.1155/2021/6687474

Yuan, M., Huang, L.-L., Chen, J.-H., Wu, J. and Xu, Q. (2019). The emerging treatment landscape of targeted therapy in non-small-cell lung cancer. *Signal Transduct. Target Ther.* **4**, 61. doi:10.1038/s41392-019-0099-9

Zhu, Q., Luo, R., Gu, J., Hou, Y., Chen, Z., Xu, F., Wang, L., Mao, W., Lu, C. and Ge, D. (2020). High CXCR4 expression predicts a poor prognosis in resected lung Adenosquamous carcinoma. *J. Cancer* **11**, 810-818. doi:10.7150/jca.36498